Phase transitions in a two-dimensional lattice gas model of orientable diatomic molecules. II. Order-disorder transitions of superantiferromagnetic and $c(2\times2)_{AF}$ phases

W. Rżysko and A. Patrykiejew
Faculty of Chemistry, MCS University, 20031 Lublin, Poland

K. Binder
Institut für Physik, Johannes Gutenberg-Universität, 55099 Mainz, Germany

(Received 10 January 2007; revised manuscript received 2 July 2007; published 8 November 2007)

The nature of phase transitions occurring in the two-dimensional spin-1 lattice model with the first- and second-nearest-neighbor interactions is studied using Monte Carlo methods. This system models the adsorption of rigid diatomic molecules (*A*-*B*) on (100) surfaces of crystals, assuming that each molecule is oriented perpendicularly to the crystal surface, and the binding energy depends on whether the *A* atom or *B* atom is adsorbed. It is shown that under the condition of a fully filled lattice, the order-disorder transition of the superantiferromagnetic (SAF) phase may occur via a continuous as well as a first-order phase transition, depending on the model parameters. The continuous order-disorder transition of the SAF phase is found to be nonuniversal. The nature of the various phase transitions is analyzed by the finite size scaling method. The application of this method is also demonstrated for the case of a second-order transition from one ordered phase to another ordered phase. We have also demonstrated that the phase diagram topology changes with the model parameters. While at low temperatures a first-order transition between the SAF phase and the $c(2\times2)_{AF}$-ordered phase corresponding to a half-filled lattice occurs, this transition line at higher temperatures may terminate either by a triple point or a tricritical point. For the latter case a phase diagram with a different type of multicritical point is suggested.

DOI: 10.1103/PhysRevB.76.195409 PACS number(s): 64.60.Cn

I. INTRODUCTION

Various lattice models have been used to study the behavior of pseudo-two-dimensional adsorbed layers formed on crystals.[1,2] In the case of simple spherically symmetric adsorbates, e.g., atoms and simple molecules such as methane, the two-state Ising model, known also as the spin-1/2 model, is often used.[1] The Ising model Hamiltonian

$$\mathcal{H}_{\mathrm{Ising}} = J\sum_{\langle ij\rangle} s_i s_j - H\sum_i s_i \tag{1}$$

can be readily mapped onto the corresponding lattice gas model Hamiltonian

$$\mathcal{H}_{\mathrm{lg}} = u\sum_{\langle ij\rangle} n_i n_j - \mu\sum_i n_i \tag{2}$$

by replacing the spin variables ($s_i=\pm1/2$) by the occupation variables [$n_i=(2s_i+1)/2=1,0$]. The coupling constant J and the magnetic field H are then related to the nearest-neighbor interaction parameter u and the chemical potential μ,[1] respectively, and the chemical potential term may also include the contribution due to the interaction of adsorbed atoms with the substrate. Of course, one can use a similar procedure to treat more complex systems involving longer-range (second- and third-nearest neighbor and so on) interactions.

Monolayers formed by spherically symmetric adsorbates on triangular lattices, like those corresponding to the basal planes of graphite, boron nitride, and lamellar dihalides, have been found to be best represented by the lattice gas Hamiltonians obtained by the appropriate transformation of the three-state Potts model Hamiltonian.[3]

When one considers adsorption of nonspherical molecules, e.g., rigid diatomic molecules (*A*-*B*), the situation becomes more complex, due to the larger number of possible configurations. The adsorbed molecule may occupy one or two lattice sites, depending on whether it assumes the orientation parallel or perpendicular to the surface.[4–6] In the latter case, one also has to distinguish between two different states, corresponding to the cases when different atoms (*A* or *B*) are in contact with the surface. In several experimentally studied systems, e.g., monolayers of CO on NaCl(100) or MgO(100) surfaces,[7–9] the adsorbed molecules are highly tilted, and preferentially adsorbed via one atom. This allows one to model such systems using the spin-1 lattice model, in which the spin variable can take upon three different values ±1 and 0,[10] depending whether a lattice site is taken by *A*, *B*, or is empty. In real adsorption systems the corrugation potential is often too weak to exclude the formation of films in which the adsorbed atoms assume the positions other than resulting from the surface lattice structure. But we assume throughout that the corrugation potential of the substrate is so strong that adsorption occurs only on the sites of the "preferred lattice" defined from the minima of this potential, and hence lattice models are an appropriate description of the system.

Several versions of the spin-1 lattice model have been proposed[10–17] and applied to study a variety of problems in condensed matter physics: the description of one and multicomponent fluids,[13–15] dipolar and quadrupolar orderings in magnets,[16,18] microemulsions,[12] ordering in semiconducting alloys,[19] and adsorbed layers.[4–6,20,21] The model proposed by Blume, Emery, and Griffiths (BEG)[13] was quite successfully used to describe the phase behavior of liquid helium mixtures, consisting of ^{3}He and ^{4}He isotopes.

 ©2007 The American Physical Society

The interest in spin-1 lattice models stems not only from their possible applications to describe diverse physical systems, but is also highly stimulated by the observed richness of their phase diagrams. Already in the case of spin-1 lattice models involving the first-nearest neighbor interactions only, different types of ordered phases and several different phase diagram topologies have been found.[13,14,22,23] A complex phase behavior of spin-1 lattice models primarily arises from competing interactions involving, in the most general case, the bilinear, biquadratic, and quadrilinear first-nearest-neighbor interactions and linear as well as quadratic single spin terms, which describe the effects due to the single spin anisotropy and the external field.

The situation becomes still more complex when the second-nearest-neighbor interactions are taken into account.[4,24] The transfer matrix finite size scaling calculations of Badehdah *et al.*[24] suggested that in such a case a rather simple Blume-Capel (BC) model[10,11] may violate the ordinary universality hypothesis. Extensive Monte Carlo calculations, reported in our previous paper,[4] have clearly demonstrated that the extended BEG spin-1 lattice model with the first- and the second-nearest-neighbor interactions possesses a rich variety of ordered structures of different symmetry and exhibits phase diagrams of different topology, depending on the model parameters.

This paper reports on the results of the Monte Carlo simulation study of the same model, but in other regions of the parameter space. In particular, we concentrate on a series of systems which, at sufficiently low temperatures order into the $c(2\times2)_{\mathrm{AF}}$-ordered phase, corresponding to a half-filled lattice, and into the dense superantiferromagnetic (SAF) phase, corresponding to a fully filled lattice. Our primary aim here is to elucidate the effects of varying the strength of different coupling constants on the phase behavior and crossover between different universality classes of the phase transitions. It is demonstrated that SAF order-disorder transition may be either a first- or a second-order transition, and that the first-order phase transition between the low density $c(2\times2)_{\mathrm{AF}}$ and the high density (SAF) ordered phases may terminate at a triple point or at a tricritical point. In the former case we have found the peritecticlike phase diagram topology[25] at low temperatures, while in the latter case a new type of multicritical point has been observed, above the tricritical point of the $c(2\times2)_{\mathrm{AF}}$ to SAF transition.

The paper is organized as follows. In Sec. II we recall the model and define the order parameters used to monitor the formation of different ordered phases. Section III is devoted to a description of the Monte Carlo methods applied here. The results are presented and discussed in Sec. IV. The paper concludes in Sec. V, where we briefly summarize our findings.

II. MODEL

Although the applied lattice gas model is the same as used in our earlier work,[4] nevertheless it seems justified to recall its basic assumptions again. We consider a simple square lattice of sites, and to each site i we assign an occupation variable n_i, which is equal to zero (unity) when the site is empty (occupied).

Each occupied site hosts a diatomic molecule, which is assumed to take on only the vertical orientation with respect to the surface plane and can be bound to the surface via either atom A or B. The energy of adsorption depends on the orientation of the adsorbed molecule and is given by

$$V(s_i)=\begin{cases} V_A, & s_i=1 \\ V_B, & s_i=-1, \end{cases} \tag{3}$$

where the spin variable $s_i=1$ and -1 corresponds to two different orientations of the molecule adsorbed at the lattice site. Then, we assume that a pair of molecules interacts one with another, whenever they occupy the first- as well as the second-nearest-neighboring sites. The energy of interaction between a pair of molecules also depends on their relative orientation, and can be written as $u_k(s_i,s_j)$, where $k=1$ or 2 for the first- and the second-nearest-neighbor interaction, respectively. We should emphasize that for simplicity, the interaction energy is assumed to depend only on the relative orientation of both molecules, so that we can define $u_k(s_i,s_j)$ as

$$u_k(s_i,s_j)=\begin{cases} u_{k,a}, & s_i=s_j \\ u_{k,b}, & s_i\neq s_j \end{cases}, \quad k=1,2. \tag{4}$$

The Hamiltonian of the above defined model can be written as

$$\mathcal{H}=\frac{1}{2}\sum_{\langle ij\rangle_1} n_i n_j u_1(s_i,s_j)+\frac{1}{2}\sum_{\langle ij\rangle_2} n_i n_j u_2(s_i,s_j) + \sum_i V(s_i)n_i-\mu\sum_i n_i, \tag{5}$$

where the first (second) sum runs over all pairs of the first (second) nearest neighbors, μ is the chemical potential, and the sums in the third as well as in the fourth terms run over all lattice sites. Here we assume that all energies $[u_k(s_i,s_j)$ and $V(s_i)]$ are negative (positive) for attractive (repulsive) interactions.

The ground state properties of the model can be conveniently described using the parameters $\Delta V=V_B-V_A$, $\Delta u_1=u_{1,a}-u_{1,b}$, and $\Delta u_2=u_{2,a}-u_{2,b}$. Throughout this paper we assume that $|V_B|$ is taken as a unit of energy and assume that $V_A=-2.0$, $V_B=-1.0$ so that $\Delta V=1.0$. Thus the interaction energies $u_{k,l}$ ($k=1,2$ and $l=a,b$), the differences Δu_k ($k=1,2$), as well as all other energylike quantities, such as temperature and the chemical potential, are expressed in units of $|V_B|$. A particular choice of the values of the parameters V_A and V_B was made to make the results compatible with those presented in our previous work.[4]

The model predicts that when the first-nearest-neighbor interactions $u_{1,k}$ ($k=a,b$) are either attractive or repulsive while the second-nearest-neighbor interactions $u_{2,k}$ ($k=a,b$) are nonrepulsive, six different ordered structures can appear in the ground state (see Fig. 1). In the case of nonrepulsive first-nearest-neighbor interactions only the ordered states of the total density $\rho=\Sigma_i n_i^N=1$, i.e., with all N lattice sites occupied, are possible. All these structures (F, AF, SAF, and A_3B) are schematically shown in the upper part of Fig. 1. On the other hand, when the first-nearest-neighbor interactions

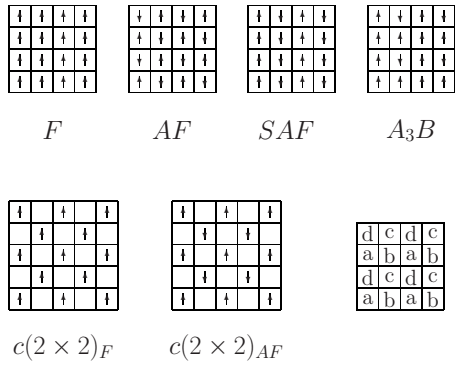

FIG. 1. Schematic representation of different possible ordered states (↑ and ↓ denotes molecules adsorbed via the atom A and B, respectively) and the decomposition of a square lattice into four equivalent sublattices a, b, c, and d.

($u_{1,a}$ and/or $u_{1,b}$) become repulsive, the two additional ordered states of the density $\rho=0.5$, in which only half of all lattice sites are occupied by the adsorbed molecules and labeled as $c(2\times2)_{\mathrm{F}}$ and $c(2\times2)_{\mathrm{AF}}$ (see lower part of Fig. 1), can also be formed. The regions of stability of the above listed ordered phases are shown in Fig. 2, which presents the ground state phase diagram evaluated for $\Delta V=1.0$.

The locations of three triple points t_1, t_2, and t_3 are entirely determined by the values of Δu_1, Δu_2, and ΔV as follows:

$$t_1: \quad \Delta u_1 = 0.25\Delta V, \quad \Delta u_2 = 0.0,$$

$$t_2: \quad \Delta u_1 = 0.5\Delta V, \quad \Delta u_2 = 0.25\Delta V,$$

$$t_3: \quad \Delta u_1 = 0.0, \quad \Delta u_2 = 0.25\Delta V. \tag{6}$$

The above lattice gas model Hamiltonian can be mapped onto the appropriate spin-1 lattice model Hamiltonian

$$\mathcal{H}' = \frac{1}{2}\bar{u}_1 \sum_{\langle ij\rangle_1} S_i^2 S_j^2 + \frac{1}{2}\Delta\hat{u}_1 \sum_{\langle ij\rangle_1} S_i S_j + \frac{1}{2}\bar{u}_2 \sum_{\langle ij\rangle_2} S_i^2 S_j^2 + \frac{1}{2}\Delta\hat{u}_2 \sum_{\langle ij\rangle_2} S_i S_j + \bar{V}\sum_i S_i^2 - \Delta\hat{V}\sum_i S_i - H\sum_i S_i^2, \tag{7}$$

where the spin variable can assume three different values $S_i=s_i=\pm1,0$, the occupation variable n_i is replaced by S_i^2,

$$\bar{u}_k = \frac{1}{2}(u_{k,a} + u_{k,b}), \quad \Delta\hat{u}_k = \frac{1}{2}(u_{k,a} - u_{k,b}), \tag{8}$$

$$\bar{V} = \frac{1}{2}(V_A + V_B), \quad \Delta\hat{V} = \frac{1}{2}(V_B - V_A), \tag{9}$$

and H is the external field, which can be related to the chemical potential μ. This spin-1 model Hamiltonian is better suited to define the order parameters representing different ordered structures because possible symmetries are easily recognized.

If one decomposes the entire lattice into four interpenetrating and fully equivalent sublattices, as shown in the rightmost panel of the lower part of Fig. 1, the average magnetization of each sublattice k (a,b,c, and d) is given by

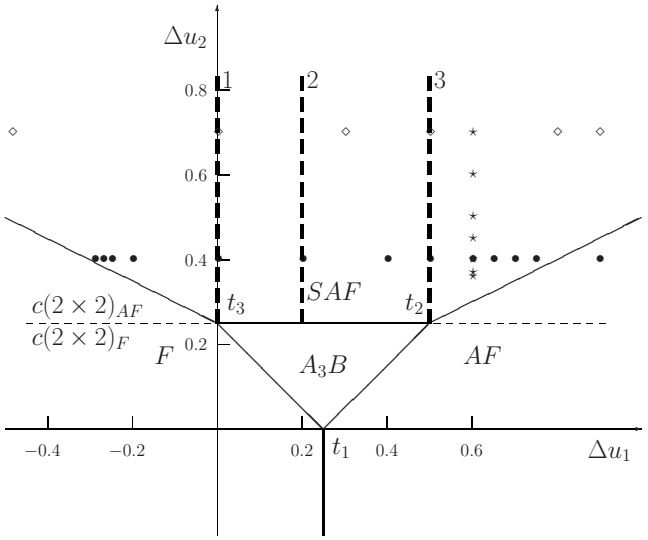

FIG. 2. Ground state phase diagram for the systems with $\Delta V=1.0$. Horizontal dashed line delimits the regions of stability of low density ordered phases $c(2\times2)_{\mathrm{F}}$ and $c(2\times2)_{\mathrm{AF}}$ and solid lines delimit the regions of stability of the ordered phases of the density $\rho=1$. Symbols (●, ◇, and ⋆) show the points at which the calculations have been carried out. Vertical thick dashed lines mark the paths considered in Ref. 4.

$$m_k = \frac{1}{L^2}\sum_{i\in k} S_i. \tag{10}$$

Of course, one can equivalently work using the lattice-gas formulation and define sublattice densities instead of the above defined sublattice magnetizations, but the use of spin variables is more convenient and simplifies the notation. One should note that the structure and symmetries of all ordered phases are quite well described by the sublattice magnetizations.

Using the above sublattice magnetizations we define the following four order parameters:

$$\Psi_1 = m_a - m_b - m_c + m_d, \tag{11}$$

$$\Psi_2 = m_a + m_b - m_c - m_d, \tag{12}$$

$$\Psi_3 = m_a - m_b + m_c - m_d, \tag{13}$$

$$\Psi_4 = m_a + m_b + m_c + m_d. \tag{14}$$

The order parameters Ψ_1 and Ψ_2 represent two components of the order parameter suitable to detect the presence of the SAF as well as $c(2\times2)_{\mathrm{AF}}$ phases. In the case of a square lattice considered here, the two components of the above order parameter are equivalent and the order parameter is invariant under global rotation. Thus it is the magnitude of the order parameter which matters, and we define the order parameter Ψ_{SAF} as

$$\Psi_{SAF} = \sqrt{\Psi_1^2 + \Psi_2^2}. \tag{15}$$

The order parameter Ψ_3 describes the ordering characteristic to AF and $c(2\times2)_F$ structures, while Ψ_4 is suitable for describing the F phase.

It is also convenient to define the order parameter, which allows one to distinguish the phases SAF and $c(2\times2)_{AF}$. Namely, by dividing the lattice into cells, each containing four sites belonging to different sublattices, the order parameter suitable for detecting the phase SAF can be defined as[33]

$$\Psi_5 = \sum_n (S_{n,a} - S_{n,c})(S_{n,b} - S_{n,d}), \tag{16}$$

where the sum runs over all cells and $S_{n,k}$ represent the spin variable of the site belonging to the cell n and the sublattice k ($k=a$, b, c, or d). The order parameter Ψ_5 is equal to zero in all phases but SAF, for which it is equal to unity.

The order parameters defined above: Ψ_{SAF}, Ψ_3, Ψ_4, and Ψ_5 suffice to distinguish all ordered phases considered in this work. Namely, we exclude from the discussion the systems, which in the ground state can order into the A_3B phase.

III. MONTE CARLO METHOD

The model presented above has been studied by Monte Carlo methods in the grand canonical ensemble,[26,27] using the simulation cell of the size $(L\times L)$, with L ranging between 20 and 140 and periodic boundary conditions are applied in both spatial directions.

In order to study the nature of different phase transitions predicted to occur in the model, we have applied the histogram reweighting method[28,29] as well as the hyperparallel tempering technique,[30,31] supplemented by the finite size scaling analysis.[27] In particular, the hyperparallel tempering allows one to investigate several thermodynamic states in a single run and, due to much faster convergence and lower fluctuations, is much less time demanding than independently performed simulations at each state point.[30] These features are of particular importance here since it has been found that in order to obtain reliable results, rather large systems were necessary.

The length of the Monte Carlo (MC) runs ranged between 10^6 and 10^7 Monte Carlo steps, where 1 Monte Carlo step corresponds to one sweep over the entire lattice.

The recorded quantities were the densities of differently oriented particles ρ_{s_i}, the total density $\rho=\rho_{-1}+\rho_1$, the above defined order parameters, which always are taken to be absolute values, the corresponding susceptibilities

$$\chi_{\Psi,L}(T) = \frac{L^2}{kT}[\langle\Psi^2\rangle - \langle|\Psi|\rangle^2], \tag{17}$$

and the fourth-order cumulants[27]

$$U_{\Psi,L}(T) = 1 - \frac{\langle\Psi^4\rangle}{3\langle\Psi^2\rangle^2}. \tag{18}$$

In the above, Ψ denotes any of the order parameters defined in Sec. II.

Apart from the above defined structural parameters we have also calculated the average energy (per lattice site), $\langle e\rangle$ and the heat capacity C_V, obtained from the fluctuation theorem

$$C_V = \frac{L^2}{kT^2}[\langle e^2\rangle - \langle e\rangle^2]. \tag{19}$$

We recall that since we have assumed ΔV to be the unit of energy, the reduced temperature is defined as $T^*=kT/\Delta V$, and the reduced chemical potential is given by $\mu^*=\mu/\Delta V$.

IV. RESULTS AND DISCUSSION

The aim of our study is twofold. In Sec. IV A we concentrate on the order-disorder transition of the SAF phase, and consider a rather special case of fully filled lattice. It is demonstrated that this phase transition can be of the first as well as of the second order, depending on the magnitude of the model parameters. It is also shown that the continuous order-disorder transition of the SAF phase is nonuniversal.

Two sets of systems have been considered, characterized by different values of the model parameters. In the first set of systems, labeled as $S1$, we have fixed the value of $\Delta u_1 = 0.6$ ($u_{1,a}=-1.0$ and $u_{1,b}=-1.6$) and changed the magnitude of Δu_2, assuming that $u_{2,a}$ is equal to 0.0, while allowing $u_{2,b}$ to vary. Thus, we have performed the calculations at the points marked by stars in Fig. 2.

In the second series of systems, labeled as $S2$, we have fixed the value of $\Delta u_2=0.4$ ($u_{2,a}=0.0$ and $u_{2,b}=-0.4$), while the magnitude of Δu_1 has been varied, between −0.29 and 0.9, assuming that $u_{1,a}$ is constant and equal to −1.0. These parameter combinations are shown by full dots in Fig. 2.

In the second part of this section (Sec. IV B) we attempt to evaluate the phase diagrams for the systems characterized by different values of the interaction parameters. It is shown that the phase diagram topology depends on the relative magnitudes of interaction energies between the pairs of differently oriented molecules. In particular, it is shown that the lines of continuous order-disorder phase transitions of $c(2\times2)_{AF}$ as well as of SAF phases meet the line of, also continuous, phase transition between the $c(2\times2)_{AF}$ and SAF at the multicritical point.

In the present paper, we have performed the calculations at the points marked by diamonds in Fig. 2. Thus, we have assumed that $\Delta u_2=0.7$ ($u_{2,a}=0.0$, $u_{2,b}=-0.7$), $u_{1,a}=0.5$, and allowed $u_{1,b}$ to vary between −0.5 and 1.0. Nine different systems, characterized by the values of $u_{1,b}$ given in Table I, have been considered.

A. Disordering of the SAF phase on a fully filled lattice

We begin with a discussion of the order-disorder transition of the SAF structure, occurring under the condition of the fully filled lattice, $\rho=1.0$. This problem has already been addressed in our previous work,[4] where we have discussed the systems with the fixed values of $u_{1,a}=-1.0$, $u_{1,b}=-1.2$ ($\Delta u_1=0.2$), and $u_{2,a}=0.0$ and different values of $u_{2,b}$ exceeding −0.25, along the path marked by a thick dashed line 2 in Fig. 2. It has been demonstrated that the critical behavior of the order-disorder transition is nonuniversal. In particular, we have found that the fixed point of the order parameter cumulant U^*_{SAF} changes with Δu_2 (see Fig. 3) and approaches a constant value of about 0.64 when Δu_2 becomes large

TABLE I. The listing of systems discussed in Sec. IV B and characterized by $\Delta u_2=0.7$ ($u_{2,a}=0.0$, $u_{2,b}=-0.7$) and different values of Δu_1 ($u_{1,a}=0.5$).

Label	Δu_1
*M*1	−0.5
*M*2	0.0
*M*3	0.3
*M*4	0.5
*M*5	0.6
*M*6	0.7
*M*7	0.8
*M*8	0.9
*M*9	1.0

enough. It has been also shown that, unexpectedly, the critical exponents γ and ν gradually approach Ising values of $\gamma=1.75$ and $\nu=1.0$ for sufficiently large values of Δu_2 and gradually increase when Δu_2 approaches the value of 0.25, which delimits the stability regions of SAF and A_3B ordered phases. We have to admit that it is not clear why the critical exponents assume the values characteristic to the universality class of the two-dimensional (2D) Ising model, while the fixed point value of the fourth-order cumulant of the order parameter has a much larger value, of about 0.64, than predicted for the 2D Ising model,[32] namely, 0.613. Figure 4 shows the changes of the fixed point value of the order parameter cumulant and of the order-disorder transition temperature with Δu_2 obtained for the set *S*1. One readily notes that for small values of Δu_2 we obtain the results suggesting that the transition belongs to the universality class of the 2D Ising model ($U^*_{\mathrm{SAF}}\approx 0.613$) and then increases when Δu_2 becomes higher.

The difference between the systems considered in Ref. 4 (cf. Fig. 3) and these discussed here, is that in the former case the SAF structure meets the region of stability of the

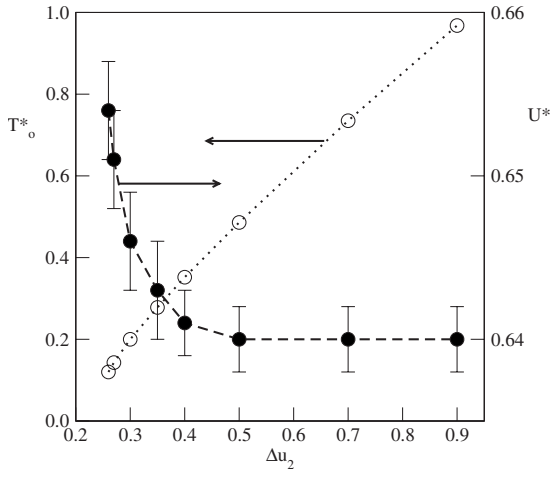

FIG. 3. The changes of the order-disorder transition temperature and of the fixed point of the fourth-order cumulant U^*, for the SAF-ordered phase, plotted against Δu_2, obtained for the systems characterized by $u_{1,a}=-1.0$, $u_{1,b}=-1.2$ ($\Delta u_1=0.2$), and $u_{2,a}=0.0$.

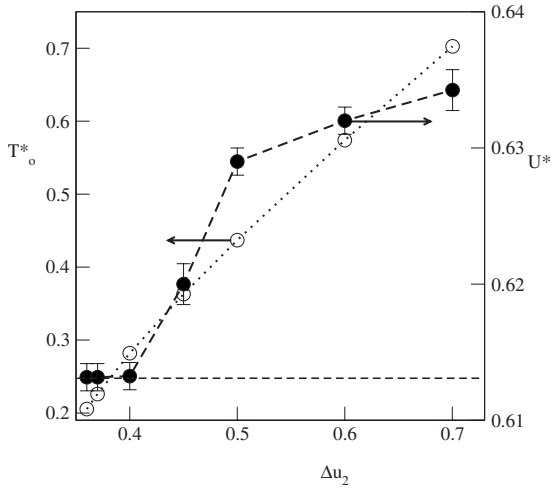

FIG. 4. The changes of the order-disorder transition temperature and of the fixed point of the fourth-order cumulant U^*, for the SAF-ordered phase, plotted against Δu_2, for the set of systems *S*1.

A_3B phase, for which the order-disorder transition is nonuniversal,[4] while in the present case the SAF structure approaches the stability region of the AF phase when Δu_2 is lowered. Although we have limited the calculations to the values of Δu_2 not larger than 0.7, nevertheless it can be anticipated that the cumulant fixed point approaches the value close to about 0.64 when Δu_2 becomes high enough, just the same as in the case of $\Delta u_1=0.2$.

The temperature of the order-disorder transition increases nearly linearly with Δu_2, just the same as in the case of $\Delta u_1=0.2$ (see Fig. 3), due to an increase of the attractive interactions in the system and a gradual departure from the point at which the structure of the ordered phase changes. In the case of the set *S*2 we have also found that the universality class of the order-disorder transition of the SAF phase changes with Δu_1 [see Fig. 5(b)].

At the present situation one might expect that the fixed point value of the order parameter cumulant approaches the

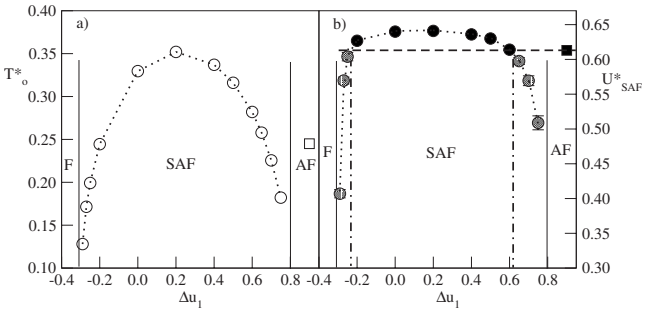

FIG. 5. The changes of the order-disorder transition temperature (a) and of the fixed point of the fourth-order cumulant U^* for the set of systems *S*2. In (b) black (gray) circles correspond to the second- (first-) order phase transitions. The second-order transition occurs in the region between the dash-dotted lines. The open square in (a) and black square in (b) mark the transition temperature and the fixed point value of the fourth-order cumulant for the order-disorder transition of the AF phase. Vertical solid lines show the stability limits of the SAF phase and the horizontal dashed line marks the value of U^* corresponding to the universality class of a 2D Ising model.

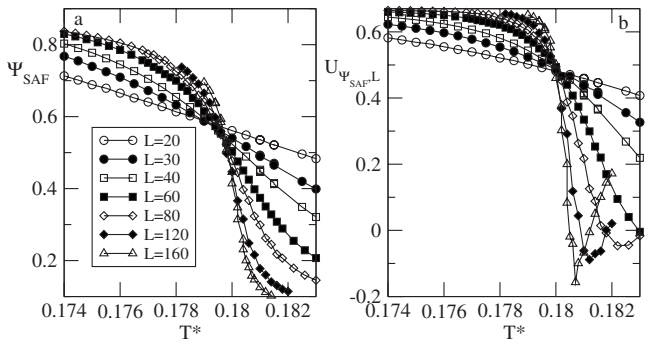

FIG. 6. Part (a) [(b)] shows the temperature changes of the order parameter Ψ_{SAF} (of the fourth-order cumulant $U_{\Psi_{SAF}}$) obtained for the system belonging to the set $S2$, with $\Delta u_1=0.75$, for different sizes of the simulation box [see legend in (a)].

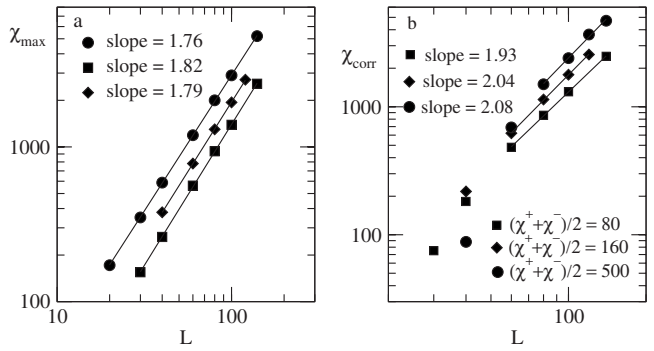

FIG. 7. Part (a) [(b)] presents the log-log plot of χ_{max} (χ_{corr}) versus simulation cell size L for two systems of the set $S2$, characterized by different values of $\Delta u_1=0.65$ (squares), 0.70 (diamonds), and 0.75 (circles).

value corresponding to the universality class of the 2D Ising model when Δu_1 becomes close to the value delimiting the stability regions of the SAF and AF phases ($\Delta u_1=0.8$) as well as the SAF and F phases ($\Delta u_1=-0.3$).

We have found, however, that it is not the case. Namely, as soon as Δu_1 exceeds about 0.60 the order-disorder transition of the SAF phase changes from continuous to discontinuous. This has been confirmed by the finite size scaling analysis of the simulation data. First, one should note that for Δu_1 exceeding 0.60, the fixed point value of the order parameter cumulant decreases monotonically and falls below the value predicted for the two-dimensional Ising model [cf. Fig. 5(b)]. Similarly, the temperature of the order-disorder transition decreases with Δu_1 and is expected to go to zero when Δu_1 approaches 0.8.

For intermediate values of Δu_1, between about −0.23 and 0.61, the transition is continuous and nonuniversal again. In particular, the fixed point value of the order parameter cumulant reaches the highest values of about 0.64 when Δu_1 is close to 0.25.

Unlike in the systems considered above, the temperature of the order-disorder transition does not change monotonically with Δu_1 [cf. Fig. 5(a)], reflecting the changes in the stability of the SAF ordered phase. Thus, it reaches the highest values for Δu_1 close to 0.25 and decreases when Δu_1 becomes lower (higher), i.e., when it gradually approaches the points at which the ordering changes from SAF to F (AF) (see Fig. 2).

However, our results demonstrated that the order-disorder transition of the SAF phase becomes a first-order transition when Δu_1 approaches the values delimiting the stability region of the SAF phase at both sides, close to the AF as well as the F phases.

The change of the nature of the order-disorder phase transition is demonstrated by the plots of temperature changes of the order parameter as well as of the fourth-order cumulants, given in Figs. 6(a) and 6(b). It is quite evident that both the order parameter as well as the fourth-order cumulant behavior is characteristic to the first-order rather than to the second-order phase transition.[34–37] In particular, the order parameters obtained for different sizes of the simulation cell exhibit a crossing point, while the cumulants show the presence of minima above the transition temperature. Such a behavior has been seen for other thermally driven first-order phase transitions, e.g., the three-state Potts model in three dimensions, and is explained by a phenomenological theory.[37]

Figure 7(a) gives the logarithmic plot of the maximum value of the order parameter susceptibility ($\chi_{SAF,max}$) versus the size of the simulation cell, L. The results suggest that the power law

$$\chi_{max}(L) \propto L^{\gamma/\nu} \tag{20}$$

is obeyed in all three cases considered and that γ/ν changes with Δu_1. If this behavior were the true asymptotic behavior, it would imply a second-order transition, with nonuniversal critical exponents. However, at first sight the first-order character of the order-disorder transition for the SAF phase in the region of Δu_1 exceeding 0.6 seems to be at variance with this conclusion, but this interpretation of the data is not unique. In fact, in the case of a first-order transition one expects that the maximum value of the susceptibility scales with the system size as[35–37]

$$\chi_{max}(L) \propto (\chi^+ + \chi^-)/2 + \alpha L^d, \tag{21}$$

where χ^+ and χ^- are the values of the susceptibility in the two coexisting phases at the transition point, and $d(=2)$ is the system dimensionality, and α is a constant. Therefore, $\chi_{corr}(L)=\chi_{max}(L)-(\chi^+ + \chi^-)/2$ scales with L as L^2. The values of $\chi_0=(\chi^+ + \chi^-)/2$ can be estimated from the plot of $\chi_{max}(L)$ versus L^2, by extrapolating the data to $L=0$. Part (b) of Fig. 7 gives the log-log plots of $\chi_{corr}(L)$ against L and demonstrates that the scaling law given by Eq. (21) is also compatible with the data, for sufficiently large L. The increase of $\chi_0$with Δu_1 suggests that χ_0 also diverges when Δu_1 approaches the value delimiting the stability region of the SAF and AF phases. These problems with $\chi_{max}(L)$ clearly show that in the judgment of the order of phase transitions special care is needed, when several orderings compete, as in our model. In addition, it should be noted that there possibly is a slight but systematic underestimation in our data for $\chi_{max}(L)$, since at a first-order phase transition the relaxation time increases exponentially with L.[27]

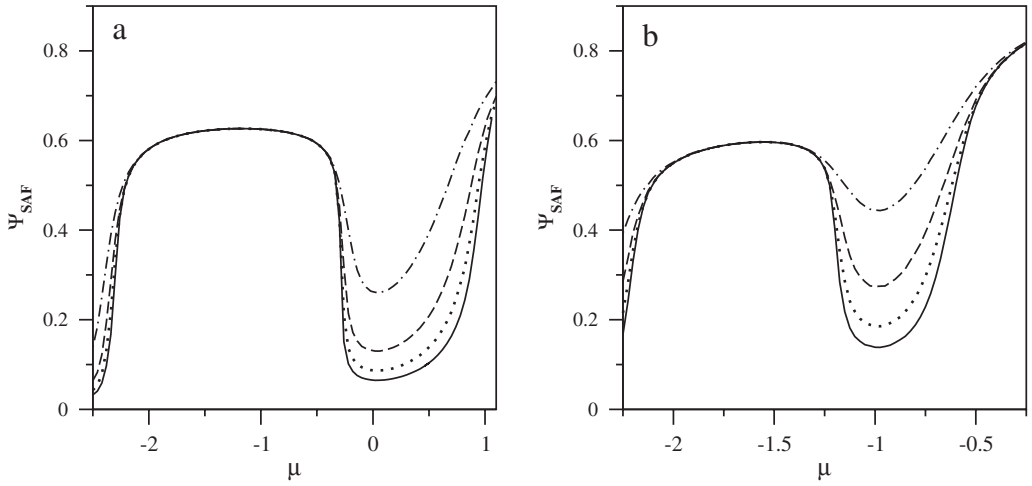

FIG. 8. The changes of the order parameter Ψ_{SAF} with the chemical potential, for the systems $M1$ (a) and $M2$ (b) calculated at the temperature $T=0.6$ for different sizes of the simulation cell, given in the figure.

Of course, when Δu_1 exceeds the value of 0.8, the ordering changes and the stable ordered state is the AF phase, which exhibits the continuous order-disorder transition belonging to the universality class of the 2D Ising model at least if Δu_1 exceeds the transition values (0.8) enough. This is confirmed by the data given in Fig. 5. On the other hand, when Δu_1 becomes lower than -0.3 we enter the stability region of the F phase. Under the condition of a fully filled lattice this phase disorders gradually, as was demonstrated in our previous work.[4]

B. Phase behavior of systems involving the $c(2\times2)_{AF}$ phase

Now, we turn to the discussion of the systems, in which the first nearest-neighbor interaction between a pair of molecules with the same orientation is repulsive. Under such a condition the model predicts the formation of one of the ordered phases of the density $\rho=0.5$ [$c(2\times2)_F$ and $c(2\times2)_{AF}$], depending on the magnitude of Δu_2, prior to the formation of dense ordered phases (F, AF, A_3B, or SAF). Similarly to the previously discussed systems, we assume that both Δu_1 and Δu_2 are such that the fully occupied lattice orders into the SAF phase at sufficiently low temperatures. It should be mentioned here that two series of systems, for which the low density ordered phases $c(2\times2)_F$ and $c(2\times2)_{AF}$ appear, have been already discussed in Ref. 4. In particular, we have considered the changes of the model phase behavior with Δu_2, for two different values of Δu_1 equal to 0.0 and 0.5, along the paths marked by thick vertical dashed lines 1 and 3 in Fig. 2.

Here we present the results obtained for the systems characterized by the parameters listed in Table I. For the assumed values of the interaction parameters the model predicts that at sufficiently low temperatures, the condensation occurs via two first-order phase transitions. The first transition occurs between a dilute gas and the ordered $c(2\times2)_{AF}$ phases,

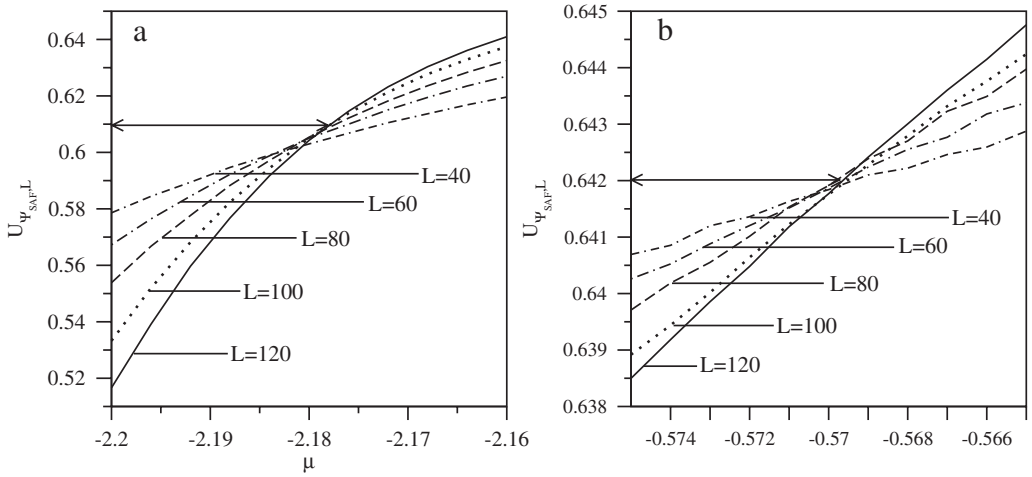

FIG. 9. The changes of the fourth-order cumulants $U_{\Psi_{SAF},L}$ with the chemical potential, for the system $M2$, calculated at the temperature $T=0.6$ for different sizes of the simulation cell, given in the figure. The data given in (a) corresponds to the order-disorder transition of the $c(2\times2)_{AF}$ phase, while (b) corresponds to the order-disorder transition of the SAF phase.

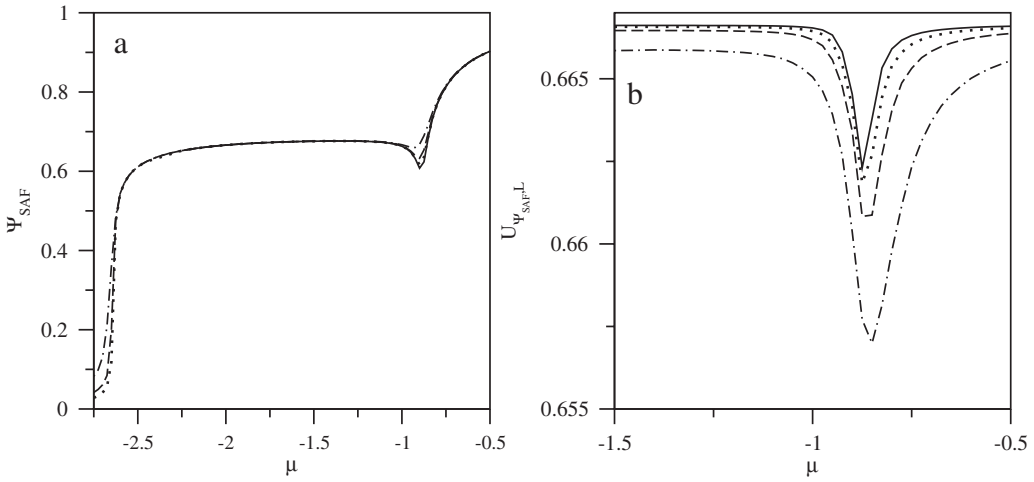

FIG. 10. (a) shows the changes of the order parameter Ψ_{SAF} with the chemical potential, for the system $M2$ at $T=0.50$, obtained for a different size of the simulation cell (shown in the figure). (b) gives the corresponding changes of the fourth-order cumulants $U_{\Psi_{\mathrm{SAF},L}}$ in the region where the disordering of the $c(2\times2)_{\mathrm{AF}}$ and the formation of the SAF phases was expected to occur. (c) shows the phase diagram topology resulting from the analysis of the simulation data for Ψ_{SAF} and $U_{\Psi_{\mathrm{SAF},L}}$.

while the second transition occurs between the $c(2\times2)_{\mathrm{AF}}$ phase and the SAF phase. In the particular case of the system $M1$, we have found that these first-order transitions terminate at the temperatures equal to about 0.45 [gas-$c(2\times2)_{\mathrm{AF}}$] and 0.395 [$c(2\times2)_{\mathrm{AF}}$-SAF], respectively.

Figures 8(a) and 8(b) present the changes of Ψ_{SAF} with the chemical potential for the systems $M1$ [(a)] and $M2$ [(b)] calculated at the temperature $T=0.6$, i.e., above the temperature range at which the first-order transitions occur, and obtained for different sizes of the simulation cell. One readily notes that the data presented indicate that there are three second-order phase transitions present in both systems. This conclusion is evident from the fact that the (absolute values of) the order parameters are rather large for small L in the disordered region near the transition, but decrease monotonously with increasing L, and no crossing points occur. The first two transitions correspond to the disordering of the $c(2\times2)_{\mathrm{AF}}$-ordered phase (at low and high density regimes), and hence are expected to be of the same nature. We have found that both transitions belong to the universality class of the 2D Ising model [see Fig. 9(a)]. On the other hand, the third transition, occurring between the disordered phase and the SAF-ordered phase, is nonuniversal [see Fig. 9(b)]. As is well known the SAF phase belongs to the universality class of the 2D XY model with cubic anisotropy,[38] which is known to have nonuniversal critical exponents. In particular, the fixed point value of the fourth-order cumulant of the order parameter is equal to about $U^{*}_{\mathrm{SAF}}=0.642$ for the system $M2$.

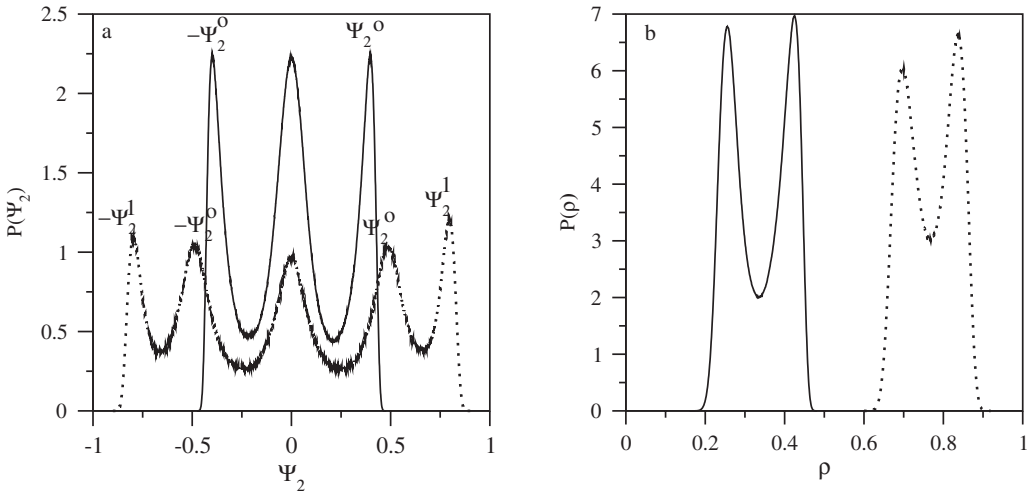

FIG. 11. (a) shows the distributions of the component Ψ_2 (the distribution of the component Ψ_1 is the same) of the order parameter Ψ_{SAF} obtained at the transition points between the dilute gas and the $c(2\times2)_{\mathrm{AF}}$ phases, for the system $M2$, at $T=0.43$ and $\mu=-2.770\,075$ (solid line), and between the $c(2\times2)_{\mathrm{AF}}$ and SAF phases, at $T=0.408$ and $\mu=-0.896\,3054$ (dotted line). (b) shows the corresponding density distributions, obtained at the same state points. The values of the chemical potential at the transition points have been determined to high accuracy using the histogram reweighting technique.

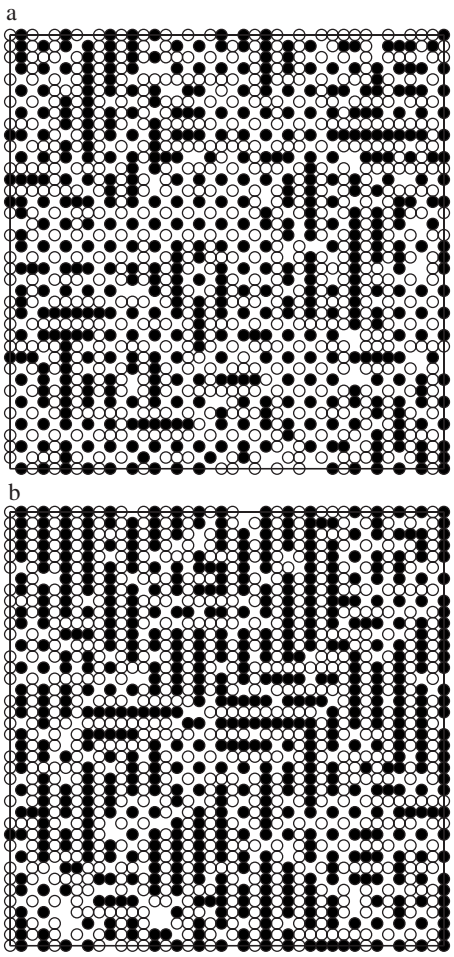

FIG. 12. Snapshots of configurations recorded at both sides of the $c(2\times2)_{AF}$ and SAF phase transition, for the system $M2$, recorded at $T=0.50$, and the chemical potentials equal to $\mu=-0.93$ (a) and -0.85 (b). Differently oriented molecules are marked by different symbols.

In the case of the system $M1$ we have obtained $U^{*}_{SAF}=0.63$. Qualitatively similar results have been found for other values of Δu_1 up to 0.8, i.e., for the systems $M3-M7$, and hence we concentrate here on the behavior of one system ($M2$).

Figures 10(a) and 10(b) show that upon the lowering of temperature to 0.5 the system phase behavior changes considerably. Although the results given in Fig. 10(a) suggest, again, that three second-order phase transitions occur, nevertheless, a finite size scaling analysis of the order parameter cumulant $U_{\Psi_{SAF}}$ detects only one phase transition, between a dilute gas and the ordered $c(2\times2)_{AF}$ phases. In particular, Fig. 10(b), which shows in enlarged scale the region in which the two other phase transitions could be expected to occur, quite clearly demonstrates that the order parameter cumulants gradually approach the trivial fixed point value of 2/3 when the system size increases. The results presented do not indicate the presence of a phase transition between the $c(2\times2)_{AF}$ and SAF phases at intermediate temperatures, between the end of the first-order coexistence and the region where there are two continuous transitions involving disordering of the $c(2\times2)_{AF}$ phase, and then the formation of the ordered SAF phase. Such a transition must occur due to the different symmetry of both phases, however.

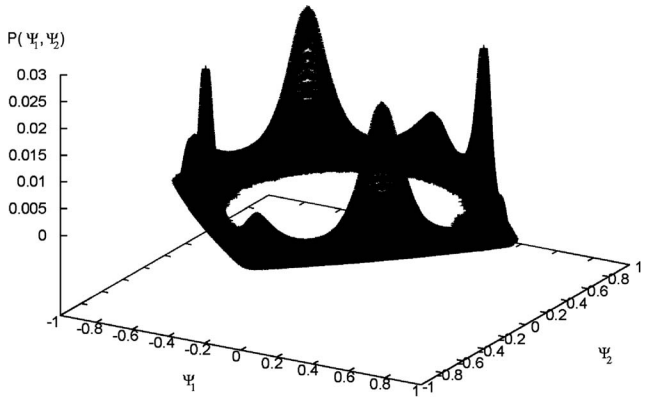

FIG. 13. Three-dimensional plot of the distribution of Ψ_1 and Ψ_2 of the order parameter Ψ_{SAF} obtained at the transition point, determined with the help of histogram reweighting technique, between the $c(2\times2)_{AF}$ and SAF phases, at $T=0.408$ and $\mu=-0.896\,305\,4$ for the system $M2$.

One should note that the order parameter Ψ_{SAF} is not suitable to distinguish between the phases $c(2\times2)_{AF}$ and SAF, and it just assumes different values, equal to 0.5 and 1.0 in perfectly ordered $c(2\times2)_{AF}$ and SAF structures, respectively. The same occurs at finite temperatures, as it is illustrated by the results shown in Fig. 11(a), where the distributions of the components Ψ_1 and Ψ_2 of the order parameter Ψ_{SAF} corresponding to the transitions between the gaslike and the $c(2\times2)_{AF}$ phases as well as between the $c(2\times2)_{AF}$ and SAF phases are presented [Fig. 11(b) shows the corresponding density distributions]. In the case of the gas-to-$c(2\times2)_{AF}$ transition the distributions of Ψ_1 and Ψ_2 exhibit the maximum at $\Psi_{SAF}=0$, corresponding to the gaslike phase, as well as two maxima at $\pm\Psi^{0}_{SAF}$, due to the $c(2\times2)_{AF}$-ordered phase. In the case of the $c(2\times2)_{AF}$-to-SAF transition, we find five maxima at the distributions of Ψ_1 and Ψ_2. Two of them, located at $\pm\Psi^{0}_{SAF}$, are due to the low density $c(2\times2)_{AF}$-ordered phase, while the remaining three maxima, two at $\pm\Psi^{1}_{SAF}$ and at $\Psi_{SAF}=0$ are due to the SAF-ordered phase. The values $\pm\Psi^{0}_{SAF}$ and Ψ^{1}_{SAF} are indicated in Fig. 11(a). The appearance of the maximum at $\Psi_{SAF}=0$ does not mark the presence of any disordered state, of course, but is a manifestation of the presence of differently oriented domains of the SAF phase. This is illustrated by the snapshots of configurations recorded at both sides of the $c(2\times2)_{AF}$-to-SAF phase transition, given in Fig. 12. It is quite well seen that the domains of the SAF phase exhibit two different orientations. This figure also shows that close to the transition point there are domains of the $c(2\times2)_{AF}$ as well as SAF ordering present. Of course, at the side of the $c(2\times2)_{AF}$ phase the contribution due to the SAF phase is rather small. Since the two components Ψ_1 and Ψ_2 of the SAF order parameter correspond to the domains oriented along two orthogonal directions, it is not possible that both of them assume zero values. Figure 13 gives the three-dimensional plot of the distribution of the order parameter components, recorded right at the transition point between

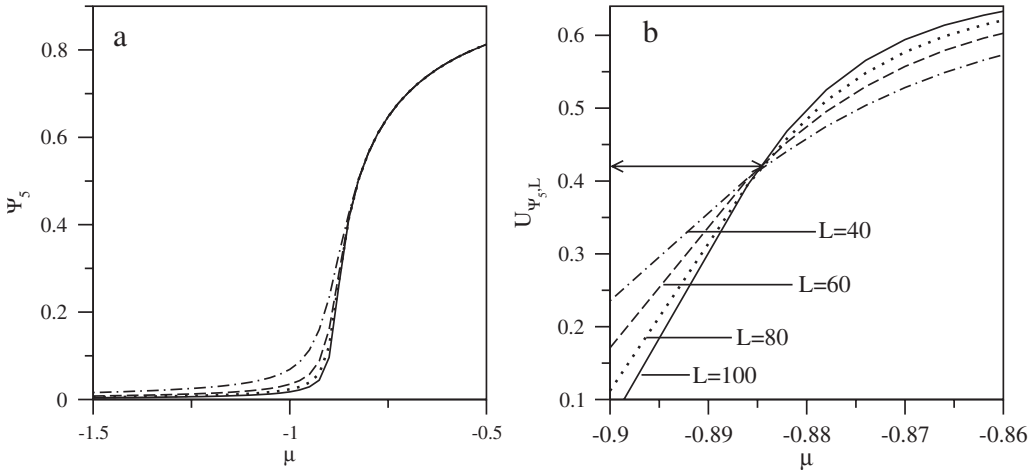

FIG. 14. (a) shows the changes of the order parameter Ψ_5 with the chemical potential, for the system $M2$, obtained for different sizes of the simulation cell (shown in the figure). (b) gives the corresponding changes of the fourth-order cumulants $U_{\Psi_5,L}$ in the region where the transition between the $c(2\times2)_{\mathrm{AF}}$ and SAF phases occurs.

the $c(2\times2)_{\mathrm{AF}}$ and the SAF phases. One observes that when one of the components is close to zero then another assumes the values close to $\pm\Psi^1_{\mathrm{SAF}}$. Since Ψ_{SAF} is not suitable to distinguish between the phases $c(2\times2)_{\mathrm{AF}}$ and SAF, its cumulant $U_{\Psi_{\mathrm{SAF}}}$ is not a useful quantity for locating a SAF $\rightarrow c(2\times2)_{\mathrm{AF}}$ transition.

On the other hand, the order parameter Ψ_5 [see Eq. (16)] is very well suited to distinguish between the $c(2\times2)_{\mathrm{AF}}$ and SAF phases, since it is finite in the SAF phase and assumes vanishing values in the $c(2\times2)$ phase. Figure 14 presents the changes of the order parameter Ψ_5 (a) and of the corresponding fourth-order cumulant $U_{\Psi_5,L}$ (b) for the same system as considered in Fig. 10. Now, it is quite evident that Ψ_5 assumes high values in the SAF phase and vanishes in the $c(2\times2)_{\mathrm{AF}}$ phase and the simulation cell becomes sufficiently large. The plots of $U_{\Psi_5,L}$ [cf. Fig. 14(b)] demonstrate that there is a continuous transition between the $c(2\times2)_{\mathrm{AF}}$ and the SAF phases.

In Table II we give the locations of the second-order phase transitions, involving the order-disorder phase transitions of both $c(2\times2)_{\mathrm{AF}}$ and SAF phases as well as the transition between the $c(2\times2)_{\mathrm{AF}}$ and SAF phases, and the fixed point values of the fourth-order cumulants (U^*_{SAF} and U^*_5).

Taking into account the above discussion and the data given in Table II we conclude that the phase diagram topology of the system discussed here is like that depicted in Fig. 15. The lines of the continuous order-disorder transitions involving the phases $c(2\times2)_{\mathrm{AF}}$ (λ_1) as well as SAF (λ_2) meet at the multicritical point, marked by the asterisk in Fig. 15. Note that we have not attempted to precisely locate the two tricritical points in Fig. 15.

The data given in Table II show that the fixed point value of the cumulant U^*_{SAF} assumes the value corresponding to the universality class of the 2D Ising model in the density region up to about 0.7. This region corresponds to the order-disorder transition of the $c(2\times2)_{\mathrm{AF}}$ phase. Then, the results obtained suggest that there exists a crossover region of density, between about 0.7 and 0.75, in which the transition changes its universality. However, our data do not allow one to precisely estimate the density at which the change of universality occurs. In particular, we cannot say whether the fixed point value of the cumulant exhibits a jump (which then presumably occurs at the multicritical point) or changes continuously (before the multicritical point is reached). One should take into account that the fixed point value of the cumulant obtained at $T=0.6$ (cf. row 5 in Table II) has been estimated using the simulation boxes of L up to 140. We have found that there are large finite size effects and the estimated crossing point of the cumulant gradually drifts toward lower values when larger and larger systems are taken into account. Therefore, it is our opinion that the true fixed point value of the cumulant should finally converge to the value characteristic of the 2D Ising model. The above statement is supported by the fact that the order parameter Ψ_5 assumes very low values and the corresponding cumulants do not exhibit a

TABLE II. The locations of (T, μ, ρ) for the second-order phase transitions at the phase diagram depicted in Fig. 15 evaluated independently using the hyperparallel tempering Monte Carlo method in grand canonical ensemble. Columns 4 and 5 give the fixed point values of its fourth-order cumulant of the order parameters Ψ_{SAF} and Ψ_5 at the transition points.

T	μ	ρ	$U_{\Psi_{\mathrm{SAF}}}{}^*$	$U_{\Psi_5}{}^*$
0.565	−2.400	0.4458	0.6100	
0.6000	−2.177	0.4735	0.6100	
0.6250	−1.876	0.5100	0.6100	
0.6250	−1.471	0.5730	0.6100	
0.6000	−1.212	0.6310	0.6250	
0.5475	−0.951	0.7300	0.6550	
0.5000	−0.884	0.7840		0.422
0.5475	−0.817	0.8100	0.6510	0.490
0.6000	−0.567	0.8775	0.6420	0.532
0.6500	−0.178	0.9270	0.641	0.545
0.7000	0.610	0.9750	0.6395	0.547

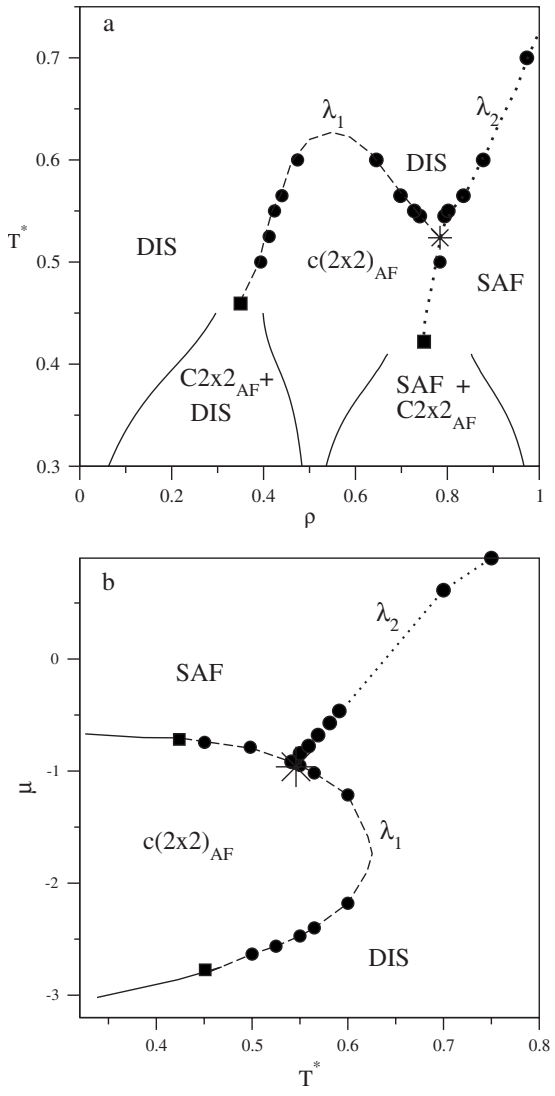

FIG. 15. The density-temperature (a) and the chemical potential-temperature (b) projections of the phase diagram obtained for the system $M2$. Solid lines represent the first-order coexistence curves while filled circles represent the locations of continuous transitions, obtained from simulation results. The dashed line λ_1 corresponds to the order-disorder transition of the $c(2\times2)_{\mathrm{AF}}$ structure, belonging to the universality class of the 2D Ising model, while the dotted line λ_2 represents the nonuniversal order-disorder transition of the SAF phase. The locations of the multicritical point are marked by an asterisk.

common crossing point at the state point considered here.

The fixed point values of the cumulants given in Table II demonstrate also that the order-disorder phase transition of the SAF phase is nonuniversal, as expected. On the other hand, the corresponding phase transition involving the $c(2\times2)$ phase belongs to the universality class of the 2D Ising model.

The data obtained for the systems characterized by different values of Δu_1 between -0.5 and 0.8 (systems $M1-M7$ suggest that in all cases the phase diagram topology is the same. In particular, the locations of the two tricritical points seem to be only weakly dependent on the magnitude of Δu_1.

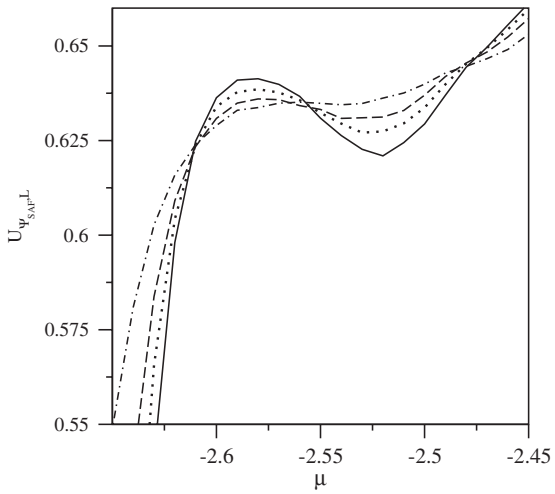

FIG. 16. The changes of the cumulants $U_{\Psi_{\mathrm{SAF},L}}$ with μ obtained for the system $M7$ at $T=0.45$ and the different size of the simulation cell (shown in the figure).

On the other hand, the maximal critical temperature decreases when Δu_1 increases. Figure 16 presents the fourth-order cumulants of the order parameter Ψ_{SAF} obtained for the system $M7$ at the temperature 0.45. It is evident that there are three order-disorder transitions present and the values of the cumulant at the intersection points differ. However, the chemical potential values, at which these transitions occur, are already very close to each other, suggesting that the temperature used is rather close to the maximal critical temperature. We should note that at the higher temperatures, above 0.5, only one phase transition, between the disordered phase and the ordered SAF phase, appears.

Figure 17 shows the variation of the fixed point values of the fourth-order cumulants of the order parameter Ψ_{SAF} corresponding to the lines λ_1, which represents the order-disorder transition of the low density ordered phase $c(2$

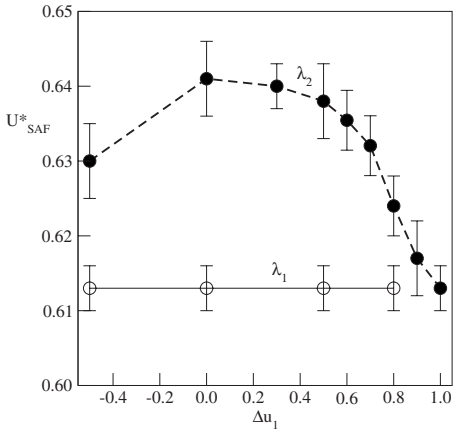

FIG. 17. The plot of U^*_{SAF} against Δu_1, along the lines of continuous transitions at $T=0.6$, evaluated for the systems $M1-M9$. Open circles represent the data for the order-disorder transition involving the low density ordered phase $c(2\times2)_{\mathrm{AF}}$, while the filled circles correspond to the order-disorder transition of the high density phase SAF.

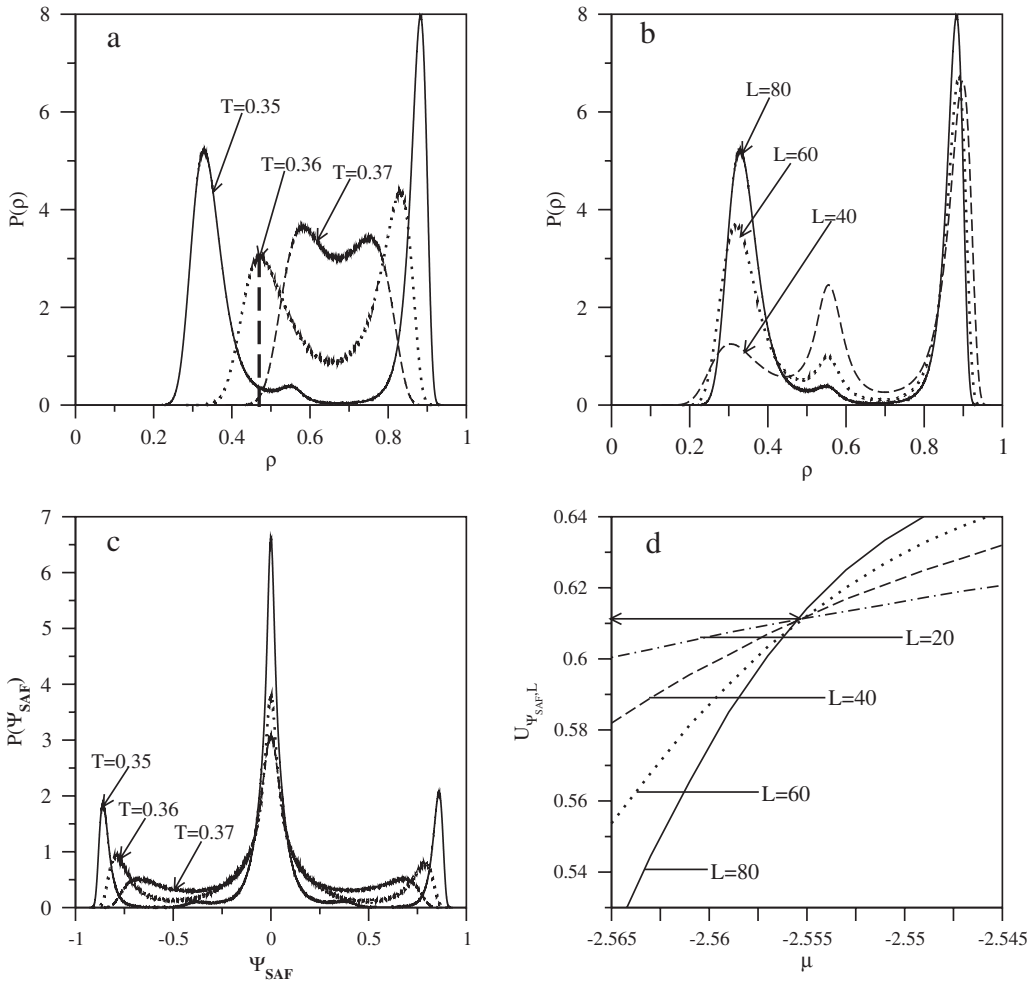

FIG. 18. (a) gives the density distributions obtained for the system $M9$, calculated along the coexistence line at different temperatures (shown in the figure) for the simulation cell with $L=80$. (b) presents a comparison of density distributions at $T=0.35$ and a different size of the simulation cell (given in the figure). (c) shows the distribution of the order parameter component Ψ_1 at different temperatures, obtained for the simulation cell size $L=80$. (d) presents the plots of the cumulants $U_{\Psi_{\mathrm{SAF},L}}$ against μ obtained for the same system at $T=0.36$ and different sizes of the simulation cell.

$\times 2)_{\mathrm{AF}}$, and λ_2, representing the disordering of the SAF phase, plotted against Δu_1. The transition represented by the line λ_1 belongs to the universality class of the 2D Ising model, while the transition occurring along the line λ_2 is nonuniversal. One should note that in the case of the order-disorder transition of the SAF phase, the behavior of U^*_{SAF} is quite similar to that shown in Fig. 5, where we have considered the same transition but in the limit of completely filled lattice and at $\Delta u_2=0.4$.

Figure 17 includes the results obtained for still larger values of Δu_1 equal to 0.9 and 1.0 (systems $M8$ and $M9$). However, in the case of the system $M9$ the phase diagram topology has been found to be different from that given in Fig. 15, as will now be discussed.

Figure 18(a) shows the examples of the density distributions evaluated at three different temperatures, close to the coexistence curve. It is well seen that the low density peak maximum at $T=0.36$ [cf. dashed vertical line in Fig. 18(a)] is located at the density equal to about 0.47, which is much higher than expected for a dilute gaslike phase and definitely much lower than expected for the high density disordered phase. Moreover, Fig. 18(a) demonstrates that the location of the low density peak is strongly temperature dependent. The maximum of this peak moves towards higher densities when the temperature increases.

One should note that at the lowest temperature used ($T=0.35$) the density distribution shows the appearance of the third, though rather small, peak at intermediate densities. This might suggest that there appears another phase, between the dilute gaslike and the high density SAF phases and that the applied temperature is close to the triple point. It appears, however, that this third maximum is only an artifact of finite size effects, as Fig. 18(b) illustrates. Although we have not performed calculations for the simulation cell larger than $L=80$, nevertheless the results presented illustrate our statement quite well. Again it is evident that easily misleading conclusions could emerge if only a single system size were examined. The inspection of snapshots recorded at $T=0.35$ for the systems of different size has demonstrated that in small systems, e.g., with $L=40$, quite large clusters corre-

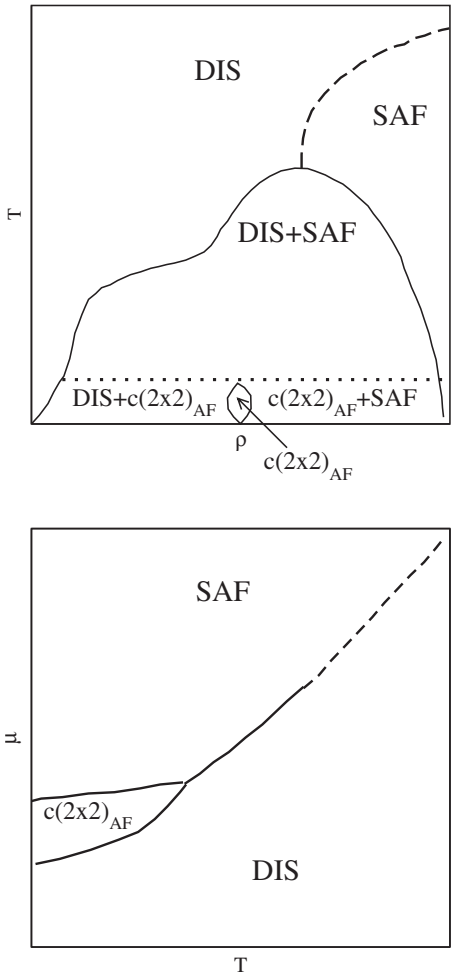

FIG. 19. Schematic representation of the phase diagram topology for the system $M9$. The horizontal dotted line shows the location of expected triple point temperature. In the particular case of the system considered here, the chemical potentials at which the gas-$c(2\times2)_{\mathrm{AF}}$ and $c(2\times2)_{\mathrm{AF}}$-SAF transitions take place at the ground state are equal to −2.15 and −1.4, respectively.

sponding to the $c(2\times2)_{\mathrm{AF}}$ structure do appear. In larger systems, we have also found such clusters, but of the sizes decreasing when the simulation cell size becomes larger.

Figure 18(c) also shows that there is only one phase transition present in the system, and that the transition corresponds to the order-disorder transition of the SAF phase. Despite the fact that the order-disorder transition of the SAF phase is nonuniversal, the order parameter cumulants fixed point assumes the value equal to about 0.612, which is practically the same as in the case of the 2D Ising model [see Fig. 18(d)].

The results of our Monte Carlo simulation suggest that the phase diagram topology is like that given in Fig. 19. Although we have not been able to find two first-order phase transitions at the low temperature region [one between the dilute gas and the $c(2\times2)_{\mathrm{AF}}$-ordered phase and another between the $c(2\times2)_{\mathrm{AF}}$- and SAF-ordered phases] due to severe problems with metastability, nevertheless their appearance can be anticipated from the ground state considerations and the fact that at finite temperatures the ordered $c(2\times2)_{\mathrm{AF}}$ phase should be stable over a finite range of densities. Our simulations have always demonstrated only the transition between the dilute gaslike phase and the dense ordered (SAF) phase.

Having the phase diagram, given in Fig. 19, the appearance of domains of the $c(2\times2)_{\mathrm{AF}}$ phase, as discussed above, can be attributed to the proximity of the triple point temperature. Note, that below the triple point temperature the system does exhibit the formation of the $c(2\times2)_{\mathrm{AF}}$ phase. When the simulation cell is small it is quite likely that large domains of this phase can appear and the system may stay in such a metastable state over a certain time. In small systems the domains of the $c(2\times2)_{\mathrm{AF}}$ phase have been found to span through the system from one side to another, and hence periodic boundary conditions stabilize such percolating clusters. The percolating clusters are less likely to appear in larger simulation cells, and hence we observe a gradual decreasing of the middle peak at the density distribution function, as shown in Fig. 18(b).

V. SUMMARY AND CONCLUSIONS

As a generic model for the phase behavior of adsorbed monolayers of orientable diatomic molecules at surfaces, the statistical mechanics of a Blume-Capel-type model on the square lattice is analyzed. This paper presents new results of Monte Carlo simulation for the spin-1 lattice model with the first- and the second-nearest-neighbor interactions, considered in Ref. 4, and we have considered two problems.

The first question concerned the nature of the order-disorder phase transition of the SAF structure, in the limiting case of a fully filled lattice. In the previous work[4] we have demonstrated that this transition is continuous and nonuniversal. It is now shown that this situation occurs only when the parameter Δu_1 is sufficiently shifted from the values delimiting the regions of stability of the SAF and AF as well as the SAF and F phases. On the other hand, when Δu_1 becomes close enough to the values at which the ground state considerations predict the change from SAF to AF as well as from SAF to F orderings the order-disorder transition of the SAF phase is of first order.

The second problem discussed in this paper concerned the changes in the phase diagram topology in the systems in which two ordered structures [$c(2\times2)_{\mathrm{AF}}$ and SAF] appear and the relative magnitudes of the first-nearest-neighbor interaction changes, while the second-nearest-neighbor interaction parameters are kept constant ($u_{2,a}=0.0$ and $u_{2,b}=-0.70$). It has been shown that the order-disorder phase transition of the $c(2\times2)_{\mathrm{AF}}$ structure is universal and belongs to the universality class of the 2D Ising model, as expected. On the other hand, the corresponding order-disorder transition of the SAF structure is nonuniversal, as demonstrated by the results given in Table II and Fig. 17. One should note that the line λ_2 presented in Fig. 17 corresponds to the SAF order-disorder phase transition at the density very close to unity, while the line λ_1, which relates to the disordering of the low density ordered structure $c(2\times2)_{\mathrm{AF}}$, has been obtained at different densities, between about 0.3 and 0.7, at which the transition

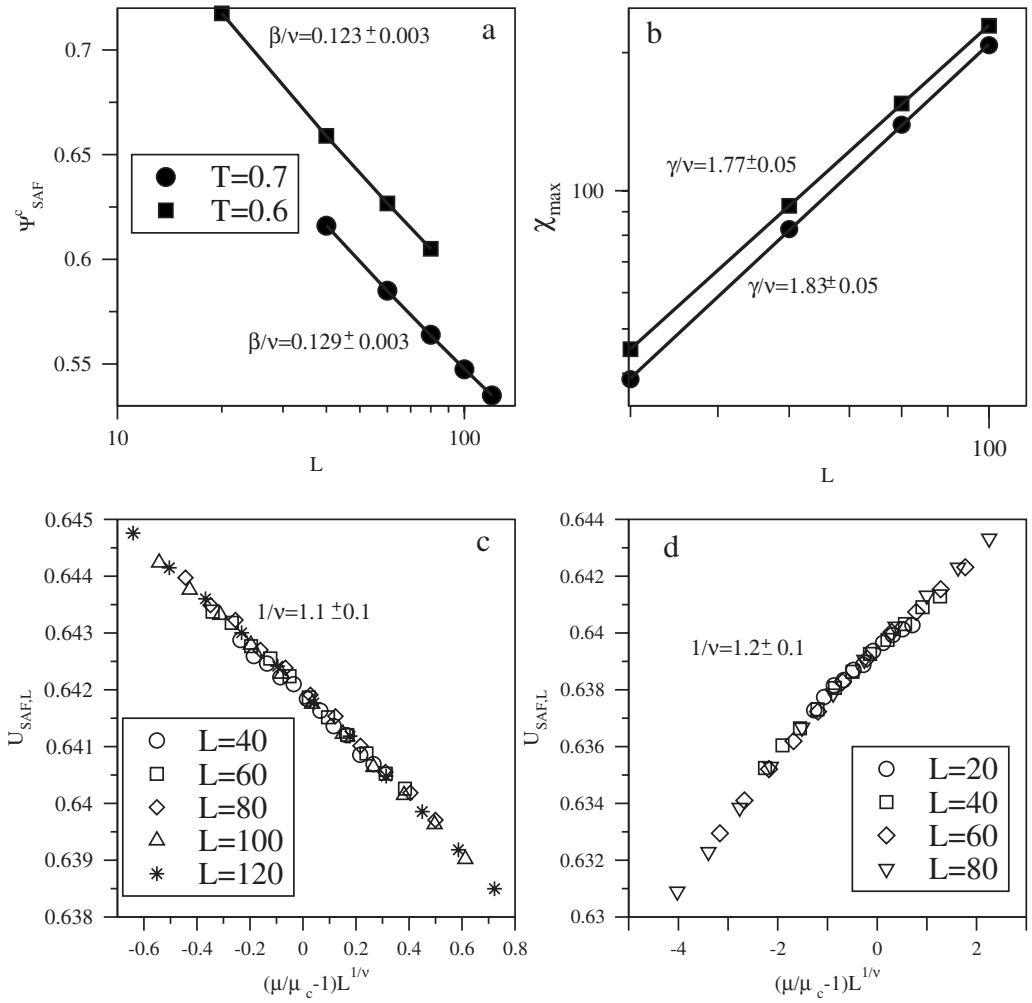

FIG. 20. (a) and (b) show the scaling plots for the order parameter Ψ_{SAF} (a) and for the conjugated susceptibility (b) for the SAF order-disorder phase transition obtained for the system $M2$ at two different temperatures [shown in (a)]. (c) and (d) show the collapsing of the fourth-order cumulants recorder for different sizes of the simulation cell (shown in the figure), also obtained for the system $M2$ at the temperatures equal to 0.6 (c) and 0.7 (d).

in question occurs. The data concerning the disordering of the SAF phase given in Table II have been obtained along the transition line (cf. Fig. 15) and hence correspond to different densities.

One of the most interesting results found in this work is the phase diagram topology for the system $M2$, depicted in Fig. 15. Namely, apart from two tricritical points we have also found a multicritical point at which the line of the continuous order-disorder phase transition of the SAF structure meets the line of critical points associated with the continuous order-disorder phase transition of the $c(2\times2)_{AF}$ structure. The order-disorder phase transition of the $c(2\times2)_{AF}$ belongs to the universality class of the 2D Ising model, while the disordering of the SAF structure is a nonuniversal transition.

We should emphasize that the accurate estimation of critical exponents associated with the second-order transitions appearing in the model is difficult due to very large corrections to scaling. Therefore, even in order to obtain reliable estimations of phase transition temperatures, using the cumulant intersection method,[27] requires very tedious calculations involving large simulation cells. Nevertheless, we have attempted to estimate the values of critical exponents characterizing the continuous order-disorder phase transition of the SAF phase (cf. the line λ_2 in Fig. 15) at two different temperatures of 0.6 and 0.7, using the finite size scaling. Figure 20 shows the log-log plots of the order parameter Ψ_{SAF} [Fig. 20(a)] and of the maximum value of the conjugated susceptibility [Fig. 20(b)] versus the simulation cell size. One notes that the values of the critical exponent ratios β/ν and γ/ν are rather close to the Ising model values, equal to 0.125 and 1.75, respectively. This result is quite consistent with the earlier study of SAF order-disorder phase transition,[39] where it was demonstrated that the nonuniversality concerns only the exponents, but not their ratios, which stay very close to the Ising values. An independent estimation of the correlation length critical exponent ν was performed using the finite size scaling of the fourth-order cumulants. Namely, the finite size scaling theory predicts that the plots of $U_{SAF,L}$ versus $L^{1/\nu}(T-T_c)$, where T_c is the temperature at which the transition takes place, for different sizes of the simulation cell should collapse at a single curve. The results obtained [see

Figs. 20(a) and 20(b)] demonstrate that $1/\nu$ is equal to 1.1 ± 0.1 ($\nu\approx0.91\pm0.09$) at $T=0.6$ and 1.2 ± 0.1 ($\nu\approx0.83\pm0.08$) at $T=0.7$. Despite rather large uncertainties the values obtained support our conclusion that the SAF order-disorder transition is nonuniversal.

It has been also shown that the phase diagram topology changes when the model parameters vary. In particular, when the parameter Δu_1 becomes high enough, the coexistence line between the ordered $c(2\times2)_{\mathrm{AF}}$ and SAF phases terminates at the triple point, leading to the so-called peritectic phase diagram topology.[25] At the temperatures higher than the triple point temperature, the transition occurs between a dilute, gaslike phase and the ordered SAF phase. We have not been able to estimate the location of that triple point temperature due to severe metastability problems. Its existence can be anticipated by considering the fact that the transition between the two ordered phases exists in the ground state ($T=0$).

ACKNOWLEDGMENTS

This work was supported by the European Community, under Grant No. MTKD-CT-2004-509249, as well as by the Deutsche Forschungsgemeinschaft under the Sonderforschungsbereich 625. One of us (W.R.) wants to acknowledge the support from the Alexander von Humboldt Foundation.

[1] K. Binder and D. P. Landau, in *Advances in Chemical Physics*, edited by K. P. Lawley (Wiley, Chichester, 1989), p. 91.
[2] A. Patrykiejew, S. Sokolowski, and K. Binder, Surf. Sci. Rep. **37**, 207 (2000).
[3] A. N. Berker, S. Ostlund, and F. A. Putnam, Phys. Rev. B **17**, 3650 (1978).
[4] W. Rżysko, A. Patrykiejew, and K. Binder, Phys. Rev. B **72**, 165416 (2005).
[5] W. Rżysko and M. Borówko, Surf. Sci. **520**, 151 (2002).
[6] W. Rżysko and M. Borówko, J. Chem. Phys. **117**, 4526 (2002).
[7] N. T. Vu, A. Jaklian, and D. B. Jack, J. Chem. Phys. **106**, 2551 (1997).
[8] D. Schmicker, J. P. Toennies, R. Vollmer, and H. Weiss, J. Chem. Phys. **95**, 9412 (1991).
[9] C. Minot, M. A. Van Hove, and J. P. Biberian, Surf. Sci. **346**, 283 (1996).
[10] M. Blume, Phys. Rev. **141**, 517 (1966).
[11] H. W. Capel, Physica (Amsterdam) **32**, 966 (1966).
[12] M. Schick and W. H. Shih, Phys. Rev. B **34**, 1797 (1986).
[13] M. Blume, V. J. Emery, and R. B. Griffiths, Phys. Rev. A **4**, 1071 (1971).
[14] J. Sivardiere and J. Lajzerowicz, Phys. Rev. A **11**, 2090 (1975).
[15] J. Sivardiere and J. Lajzerowicz, Phys. Rev. A **11**, 2101 (1975).
[16] J. Sivardiere, in *Proceedings of the International Conference on Static Critical Phenomena and Inhomogeneous Systems, Karpacz, 1984*, Lecture Notes in Physics Vol. 206 (Springer, Berlin, 1984).
[17] J. M. Yeomans, *Statistical Mechanics of Phase Transitions* (Oxford University Press, Oxford, 1992).
[18] H. H. Chen and P. M. Levy, Phys. Rev. B **7**, 4267 (1973).
[19] K. E. Newman and J. D. Dow, Phys. Rev. B **27**, 7495 (1983).
[20] T. E. Burns and J. R. Dennison, Surf. Sci. **395**, 46 (1998).
[21] T. E. Burns, J. R. Dennison, and J. Kite, Surf. Sci. **554**, 211 (2004).
[22] C. Buzano and A. Polizzola, Physica A **195**, 197 (1983).
[23] S. E. Savel'ev and G. Ramirez-Santiago, Phys. Rev. B **63**, 054424 (2001).
[24] M. Badehdah, S. Bekhechi, A. Benyoussef, and M. Tonzani, Eur. Phys. J. B **4**, 431 (1998).
[25] R. W. Cahn and P. Haasen, *Physical Metallurgy* (North-Holland, Amsterdam, 1983).
[26] M. P. Allen and D. J. Tildesley, *Computer Simulation of Liquids* (Clarendon Press, Oxford, 1987).
[27] D. P. Landau and K. Binder, *A Guide to Monte Carlo Simulation in Statistical Physics* (Cambridge University Press, Cambridge, 2000).
[28] A. M. Ferrenberg and R. H. Swendsen, Phys. Rev. Lett. **61**, 2635 (1988).
[29] A. M. Ferrenberg, in *Computer Simulation Studies in Condensed Matter Physics III*, edited by D. P. Landau, K. K. Mon, and H.-B. Schüttler (Springer-Verlag, Heidelberg, 1991).
[30] Q. Yan and J. J. de Pablo, J. Chem. Phys. **111**, 9509 (1999).
[31] T. S. Kristof and J. Liszi, Mol. Phys. **99**, 167 (2001).
[32] G. Kamieniarz and H. W. J. Blöte, J. Phys. A **26**, 201 (1993).
[33] D. Loison and P. Simon, Phys. Rev. B **61**, 6114 (2000).
[34] A. M. Ferrenberg, D. P. Landau, and K. Binder, Phys. Rev. E **58**, 3353 (1998).
[35] K. Binder and D. P. Landau, Phys. Rev. B **30**, 1477 (1984).
[36] M. S. S. Challa, D. P. Landau, and K. Binder, Phys. Rev. B **34**, 1841 (1986).
[37] K. Vollmayr, J. D. Reger, M. Scheucher, and K. Binder, Z. Phys. B: Condens. Matter **91**, 113 (1993).
[38] S. Krinsky and D. Mukamel, Phys. Rev. B **16**, 2313 (1977).
[39] D. P. Landau and K. Binder, Phys. Rev. B **31**, 5946 (1985).